East European Journal of Physics. 4. 582-589 (2025)
DOI:10.26565/2312-4334-2025-4-61 ISSN 2312-4334

MONTE CARLO CODE FOR CALCULATING THE ELASTIC AND INELASTIC SCATTERING CROSS SECTION ALONG WITH MEAN FREE PATH OF POSITRON SCATTERING IN KIDNEY, LUNG AND THYROID ORGANS

Hawar M. Dlshad[1]*, Jamal M. Rashid[2]
[1]*University of Sulaimani, College of Education, Department of Physics, Sulaymaniyah 46001, Kurdistan Region, Iraq*
[2]*University of Sulaimani, College of Science, Department of Physics, Qlyasan street, Sulaymaniyah 46001, Kurdistan Region, Iraq*
**Corresponding Author email: hawar.dlshad@univsul.edu.iq*
Received August 4, 2025; revised November 8, 2025; accepted November 15, 2025

This research calculated the total cross sections for positron scattering in kidney, lung, and thyroid tissues along an energy range of 100 eV to 1 MeV. Monte Carlo methods were employed to determine both elastic and inelastic integral cross sections, utilizing the Rutherford formula for elastic scattering and the Gryzinski excitation function for inelastic processes. A comparison was made between elastic and Penelope elastic cross sections. The study also examined elastic, inelastic, and total mean free paths as functions of positron energy for all three tissue types. The computational approach is designed to be broadly applicable across different materials. We observed significant differences in cross-section profiles and in the energy dependencies of the mean free path between tissues, attributing these variations to distinct inelastic-scattering characteristics inherent to each material. While the systematic uncertainties in the computational algorithm are challenging to quantify precisely, we believe they are largely systematic.
Keywords: *Cross section; Positron; Mean free path; Human organ; Effective atomic number*
PACS: 34.85.+x, 78.70.Bj, 87.15.-v, 34.80.Gs, 28.41.Ak

1. INTRODUCTION

A positron is defined as the electron antiparticle, having identical properties to an electron except for its positive electrical charge [1]. The interactions between positrons and electrons with solid materials form the foundation of numerous scientific and technological applications. Understanding these interactions is essential for diverse fields including microscopy, materials science, and radiation damage evaluation [2]. While extensive research has focused on electron mean free paths and cross-sections, considerably less information exists for positrons. Theoretical approaches to modeling positron scattering in solid materials can be categorized into three simple models: basic models, Boltzmann transport equation solutions, and Monte Carlo (MC) simulations. The MC technique is regarded as the most fundamental approach since it tracks individual positron paths and records complete scattering event histories. Monte Carlo simulation is a computational method with broad applications across multiple fields, including physics, biology, biophysics, nuclear engineering, biomedical engineering, and medical imaging, etc. [3, 4].

The elastic cross section in physics quantifies the probability that two particles will scatter off each other without any change in their internal states or the production of new particles. That is, the particles remain the same before and after the collision, and only their directions and/or energies may change. This differs from inelastic collisions, where particles may undergo internal transformations or give rise to additional particles [5].

Furthermore, during inelastic collisions, the target atom may be excited to a higher state above its ground level or undergo ionization, depending on the amount of energy transferred by the incident particle. Simultaneously, the incoming particle experiences energy loss and deflects away from its original trajectory. In positron emission tomography (PET) modeling, it is important to consider both positron and electron total cross sections, since high-energy positrons generate secondary electrons via ionization processes [6, 7] .

The inelastic mean free path (IMFP), which represents the mean distance a positron travels before losing energy, is crucial to surface spectroscopy techniques such as photoemission. Additionally, it plays a key role in understanding positron interactions with condensed matter, making it significant for radiotherapy planning and research on radiation effects in human tissues [8]. Ashley developed a theoretical approach to determine both the stopping power (loss of energy per unit distance) and the electrons inelastic mean free path for the range of energies up to 10 keV, based on the optical properties of the medium. This model accounts for exchange interactions between the incoming electron and the electrons of the medium [9].

The study by Tan et al. computed inelastic electron cross sections in DNA by applying the theory of dielectric response and the Penn statistical approximation, with exchange corrections accounted for. To verify their model, their calculations were evaluated by comparison to available experimental and theoretical findings, confirming the validity of their approach [10]. In the same year, they established systematic formulas to calculate both stopping powers and mean free paths of electron for numerous organic compounds, covering the range of energy below 10 keV [11]. Cai et al. determined the elastic cross sections for positrons and electrons using partial wave analysis. The inelastic interactions between positrons and valence electrons were presented by the energy loss function derived from the theory of dielectric.

Cite as: H.M. Dlshad, J.M. Rashid, East Eur. J. Phys. 4, 582 (2025), https://doi.org/10.26565/2312-4334-2025-4-61
© H.M. Dlshad, J.M. Rashid, 2025; CC BY 4.0 license

Additionally, the interactions between positrons and core electrons were represented using the excitation function of Gryzinski [12]. In this study, we systematically calculated the cross section (σ) and mean free path (λ) within the domain of energy between 100 eV to 1 MeV for three human tissues: kidney, lung, and thyroid. The calculation of total mean free paths (MFPs) for positrons is inversely related to the total scattering cross section. Additionally, the elastic cross section findings were compared with the results obtained from Penelope (2012).

2. METHODOLOGY

2.1 Cross section calculation

The overall cross section consists of two primary components: elastic and inelastic collision cross sections. The inelastic component can be further broken down into cross sections for excitation and ionization processes [10].

2.1.1 Elastic cross section

It represents scattering events where positrons interact with atomic nuclei or bound electrons without losing energy, conserving their kinetic energy while changing direction [13]. The cross section is fundamentally a microscopic parameter derived from quantum mechanical principles. When computing the positron scattering cross sections in human tissues, the model of Rutherford total elastic scattering cross section σ_{el} for atoms is employed, which can be expressed as [2]:

$$\sigma_{el} = \frac{\pi\, e^4 Z^2}{4\,\beta_N(1+\beta_N)E^2}\ , \tag{1}$$

In Eq. (1), E, Z and e are positron energy before collision in electron volts, atomic number of the target, and electronic charge, respectively. β_N is an atomic screening parameter of the Wentzel type due to Nigam et al. and is given by [14, 15]:

$$\beta_N = \frac{5.43\, Z^{2/3}}{E}\ , \tag{2}$$

It can be written as [16]:

$$\sigma_{el} = \frac{6.56\times 10^{-14} Z^2}{4\,\beta_N(1+\beta_N)E^2}\,. \tag{3}$$

In which the value of $\pi\, e^4$ is equal to $6.56\ \times\ 10^{-14}$, if the unit of E in eV and e in units of elementary charge ($1/4\pi\epsilon$). In each compound, an effective atomic number Z_{eff} must be used instead of Z atomic number, therefore Z_{eff} obtained from the Markowicz-Van Grieken expression, which is given by [17 - 19]:

$$Z_{eff} = \frac{\sum_{i=1}^{l} \frac{w_i Z_i^2}{A_i}}{\sum_{i=1}^{l} \frac{w_i Z_i}{A_i}} \tag{4}$$

Where w_i , A_i are the weight fraction given in Table (1), and atomic weight for ith element, respectively.
After each elastic collision, the scattering angle is determined using a uniform random number R, where ($0 < R \leq 1$).

2.1.2 Inelastic cross section

Represents interactions where positrons lose energy to the medium surrounded by coulomb collisions through atomic excitation and ionization mechanisms based on the classical binary-encounter theory [13]. According to Gryzinski's excitation function, the differential cross-section for an energy transfer from a positron with an energy E to an electron of the kth inner shell is [20]:

$$\frac{d\sigma}{d\Delta E} = \frac{6.56\times10^{-14}(cm^2eV^2)Z^2N_S}{(\Delta E)^3}\frac{E_B}{E}\left(1-\frac{\Delta E}{E}\right)^{\left(\frac{E_B}{E_B+\Delta E}\right)}\left(\frac{E_B}{E+E_B}\right)^{\frac{3}{2}}\left\{\frac{\Delta E}{E_B}\left(1-\frac{E_B}{E}\right)+\frac{4}{3}ln\left[2.7+\left(\frac{E-\Delta E}{E_B}\right)^{\frac{1}{2}}\right]\right\}, \tag{5a}$$

The total inelastic scattering cross-section can be calculated from:

$$\sigma_{inel} = \int_0^E \frac{d\sigma(\Delta E)}{d\Delta E}\, d\Delta E, \tag{5b}$$

Therefore

$$\sigma_{inel} = \frac{6.56\times10^{-14}}{E_B^2}\frac{N_s}{U}\left(\frac{U-1}{U+1}\right)^{3/2}\times\left[1+\frac{2}{3}\left(1-\frac{1}{2U}\right)ln\left(2.7+(U-1)^{1/2}\right)\right]. \tag{5c}$$

Here, $U = \frac{E}{E_B}$ (E_B, and ΔE are mean binding energy, and energy loss, respectively). N_s is the electrons number in a particular shell and is given for compounds as follow [2]:

$$N_s = \sum_i (\eta_{si} \times V_i) / \sum_i V_i \ . \tag{5d}$$

Where η_{si} is the electrons number in an atom particular shell of the ith species and V_i is the atoms number in ith species. Now, the total (integrated) cross sections as a function of particle energy E, can be represented as follows:

$$\sigma_{Total}(E) = \sigma_{el}(E) + \sigma_{inel}(E) + \sigma_{br}(E)[\sigma_{an}(E)] \ . \tag{6}$$

Where σ_{el}, σ_{inel}, σ_{br} and σ_{an} are elastic, inelastic, bremsstrahlung and positron annihilation cross sections respectively. Since the final term magnitude quantities (Bremsstrahlung and annihilation terms) are very small (in the order of 10^{-16}) compared to others, they can be neglected in the current calculations [21].

2.2 Mean free path calculation

Mean free path is the typical distance between collisions as a positron moves through matter. Positrons, like electrons, have both elastic and inelastic types of mean free path [22, 23]. The mean free path (λ) between interactions of the penetrating particle is expressed with [6]:

$$\lambda = \frac{A}{N_A \rho \sigma} . \tag{7}$$

Where Avogadro number N_A= 6.02214129×10^{23} mol^{-1}, ρ is the mass density (g/cm^3), and A, σ are the molar mass in unit of (g/mol) and the collision cross-section in (cm^2), respectively.

2.2.1 Elastic mean free path

The elastic form of mean free path (λ_{el}) refers to the average distance a positron travels before its direction of motion is significantly altered by an elastic collision (no energy loss) [6, 15].

$$\lambda_{el} = \frac{1}{\mathcal{N} \sigma_{el}} \tag{8}$$

$\mathcal{N}$ is the number density of molecules, given by [21, 24]:

$$\mathcal{N} = \frac{N_A \rho}{A} . \tag{9}$$

2.2.2 Inelastic mean free path

The inelastic mean free path indicates the typical distance a positron passes through before undergoing an inelastic collision, usually through processes like atomic excitation or ionization of surrounding atoms. Whether for an electron or a positron, this mean free path is inversely related to the total inelastic scattering cross section [25].

$$\lambda_{inel} = \frac{1}{\mathcal{N} \sigma_{inel}} \tag{10}$$

For penetrating positron (interaction process), the inverse of total mean free path is [2, 21].

$$\lambda_{int}^{-1} = \mathcal{N} \sigma_{int} \ . \tag{11}$$

Where λ_{int} , σ_{int} are mean free path and cross-section of interaction, respectively.

$$\frac{1}{\lambda_T} = \frac{1}{\lambda_{el}} + \frac{1}{\lambda_{inel}} , \tag{12}$$

Therefore,

$$\frac{1}{\lambda_T} = \frac{N_a \rho}{A} (\sigma_{el} + \sigma_{inel}) . \tag{13}$$

Where λ_{el}, λ_{inel}, λ_T are elastic, inelastic, and total mean free path of positron. Finally, the mean free path is crucial for understanding positron transport in materials and designing experiments using positron beams. It has many applications like: Positron annihilation spectroscopy, material defect analysis, surface studies, and thin film characterization.

3. MONTE CARLO PROCEDURE

This arduous and challenging work relied on the Monte Carlo method of probability, where a comprehensive program was developed in Visual Basic language based on the basic equations of interactions and enhanced the code with Python programming language. Information about the target substance and the energy of the interacting particle was entered as input data, considering all possible interaction probabilities at normal angles perpendicular to the target. Normally one particle trajectory was calculated in the simulation for each compound. The positrons were followed until they slowed down to an energy of 100 eV, depending on the incident energy this required few minutes. We relied on

reliable sources by entering the density value of the material and the Z values for all the compound elements, in addition to their concentrations within that compound, the atomic weight of the elements must be input. In addition to the excitation energy for each core and valence and the number of electrons in both core and valence has been entered, in which these values were taken from international tables. First, the beta values (β_N) mentioned in Eq. (2) must be calculated, and then the elastic cross section σ_{el} values and mean free path elastic λ_{el} must be calculated from Eq. (3) and Eq. (8) for each element in the compound. The inelastic cross section σ_{inel} for both core and valence are then calculated for each element in the compound, in addition to the mean free path λ_{inel} for two states of core and valence. Finally, the total mean free path λ_T is calculated by adding elastic λ_{el} and inelastic λ_{inel} as mentioned before.

4. RESULTS AND DISCUSSIONS

The purpose of this study is to present approximate calculations of cross sections and mean free paths for three types of human tissue: kidney, lung, and thyroid. We applied our method to these tissues as targets because they have wide applications in the field of Nuclear Medicine. The kidney plays a crucial role in positron emission tomography (PET) imaging and radiopharmaceutical metabolism (where (PET) is a nuclear imaging technology that allows imaging of metabolic activities of body tissues or organs) [26, 27]. Lungs are also important in positron scattering research because their low density affects attenuation correction and positron range, influencing PET image resolution and disease diagnostics such as cancer and fibrosis. The thyroid gland is also significant in PET imaging and radiation dosimetry due to its unique physiological and metabolic properties [28]. The composition of materials for each kidney, lung, and thyroid tabulated in Table 1.

Table 1. Material composition of Kidney, Lung and Thyroid [29 - 31]

Fraction by weight			
Element	**Kidney**	**Lung**	**Thyroid**
H	0.103	0.103	0.104
C	0.132	0.105	0.119
N	0.03	0.031	0.024
O	0.724	0.748	0.745
Na	0.002	0.002	0.002
P	0.002	0.002	0.001
S	0.002	0.003	0.001
Cl	0.002	0.003	0.002
K	0.002	0.002	0.001
Ca	0.001	-	-
I	-	-	0.001
Density$\boldsymbol{\rho}$ (g/cm^3)	1.05	1.05	1.05

4.1 Scattering cross sections

These graphs show how positron interaction cross sections vary with energy in kidney, lung, and thyroid tissue from 100 eV to 1 MeV. The semi-logarithmic plots display four interaction mechanisms with cross section (cm²) on the y-axis and positron energy on the x-axis. In all three graphs, the red dashed lines represent the calculated elastic cross section, the blue lines show the calculated inelastic cross section, and the green lines are the total cross sections that calculated by the Monte Carlo (MC) method (current method), which is the sum of the total elastic and total inelastic cross sections. Moreover, the red solid line describes the Penelope elastic cross section.

Figure 1. (a) Shows positron interaction cross sections for kidney tissue, exhibiting a strong inverse relationship with energy, decreasing rapidly from 100 eV to 1 MeV. At low energies (100-1000 eV), elastic scattering (red dashed line) dominates with cross sections around 5×10^{-15} cm². At intermediate to high energies (>1000 eV), inelastic processes (blue line) become dominant. The total cross section (green line) represents the sum of all interactions, reaching 8×10^{-15} cm² at 100 eV. The Penelope elastic cross section (red solid line) appears smaller but shows minimal differences from the calculated elastic cross section due to the logarithmic scale.

Figure 1. (b) shows positron interaction cross sections for lung tissue. At low energies (100-1000 eV), elastic scattering dominates, while at higher energies (>1000 eV), inelastic processes become more significant. All cross sections decrease with increasing positron energy, typical for charged particle interactions with matter.

Figure 1. (c) presents positron interaction cross sections for thyroid tissue. At low energies (100-1000 eV), elastic scattering dominates with values reaching approximately (8×10^{-15} cm²). Although inelastic cross section remains a significant contributor. Above 10 keV, both elastic and inelastic cross sections converge toward negligible values. The total cross section (green line) decreases by approximately four orders of magnitude across the studied energy range. This has important implications for positron transport and dose deposition in thyroid tissue.

For all the above graphs, the comparison between the calculated elastic cross section, and the Penelope elastic cross section shows excellent agreement at higher energies but some divergence appears at lower energies. One can observe that, the largest uncertainties occur at low energies (<1000 eV), while at energies above (10,000 eV), both models agree

very well. Moreover, the greatest discrepancy between models is for thyroid tissue. These differences are most likely due to physical approximations, model assumptions, or parameterizations. And at low energies, the elastic cross section model consistently predicts higher values than Penelope. According to clinical implications the rapid decrease in cross sections with energy means that low-energy positrons interact much more frequently with kidney tissue, leading to higher local energy deposition. This is crucial for: Dosimetry calculations in PET imaging, understanding positron range and annihilation patterns [32], optimizing radiopharmaceutical design for kidney-targeted procedures.

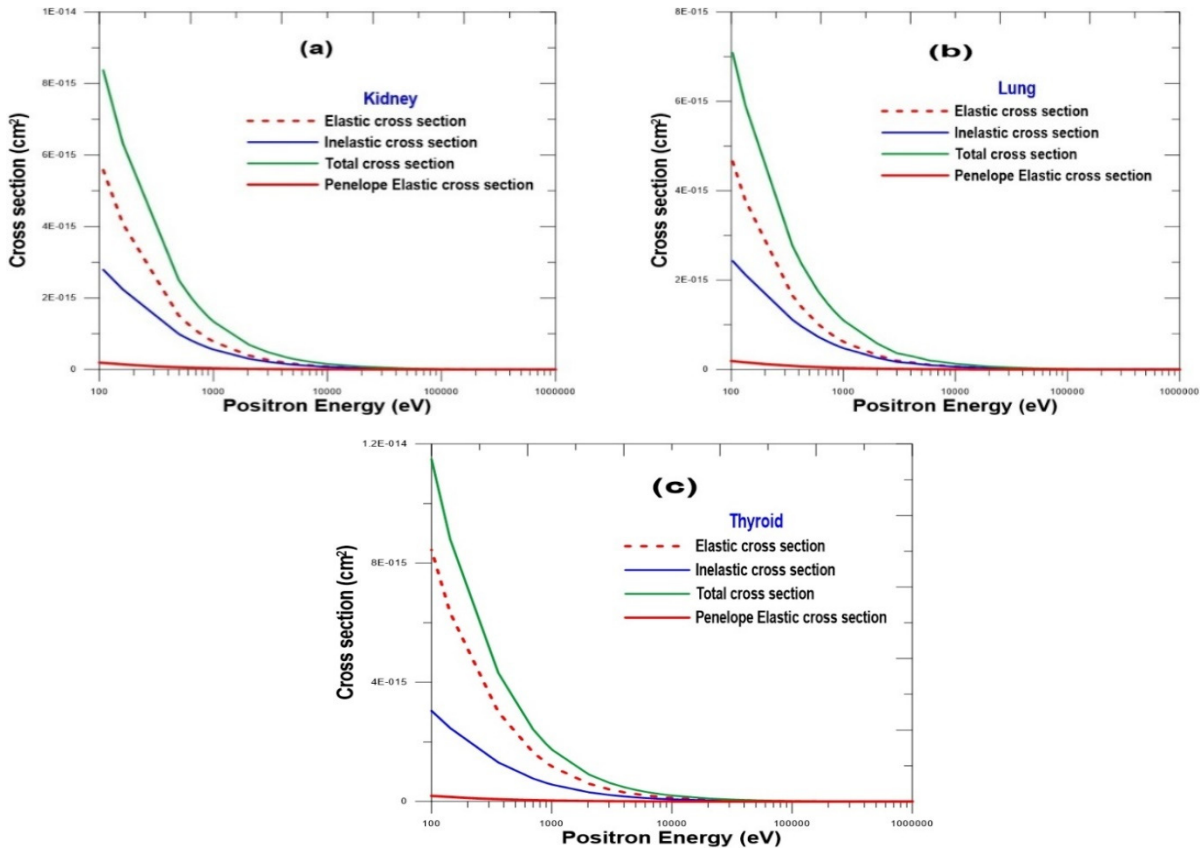

Figure 1. Calculated Elastic, Inelastic, and Total Cross section for (a): Kidney, (b): Lung, and (c): Thyroid organ. Compared with Penelope 2012 Total Elastic cross section

4.2 Positron Mean free path

Figure 2. illustrates the mean free path (in cm) for positrons in kidney, lung, and thyroid tissues plotted against positron energy (in eV). The graphs distinguish between three types of mean free path: elastic, inelastic, and total. The (blue line) represents the elastic mean free path, (red line) shows the inelastic mean free path, and the total mean free paths in (green line).

Figure 2. (a) The mean free path curves for kidney tissue inversely reflect the cross-section data from the previous section, confirming the fundamental relationship in Eq. (10). The mean free path increases dramatically with energy (roughly four orders of magnitude from 1,000 eV to 100,000 eV), explaining why low-energy positrons are effectively contained within small tissue volumes while high-energy positrons can travel much farther before interacting. The nearly identical elastic and inelastic curves indicate both scattering mechanisms are equally probable in kidney tissue. The total mean free path remains below either individual component as it combines both interaction types. This data is valuable for renal PET imaging and therapeutic applications requiring precise positron transport understanding for accurate dose calculations and image reconstruction.

Figure 2. (b) The very short mean free paths at low energies (scale of nanometer) indicate that positrons with low-energy interact very frequently with lung tissue, making them suitable for surface-sensitive applications. Higher-energy positrons penetrate much deeper before interacting. We can say, at lower energies (1,000 to 10,000 eV), the elastic and inelastic scattering have similar magnitudes. But, at energies exceeding (100,000 eV), their difference grows markedly.

Figure 2. (c) Like kidney and lung tissues, all three mean free paths in thyroid tissue increase exponentially with energy of positron, following the same principles of general physics. The one important point is that, the thyroid data shows consistently shorter mean free paths along all energies compared to kidney and lung. At high energies (over 100,000 eV), thyroid values reach about (8×10^{-6} cm) in contrast to lung values of about (1.2×10^{-5} cm). This difference is due to the higher density of thyroid compared to other tissues. Kidney, lung contain significant air spaces, making them less dense than solid thyroid. This shortest mean free paths in thyroid tissue mean positrons interact more frequently and

penetrate less deeply, which is crucial for thyroid imaging and the therapy planning of radioiodine. This data is important for accurate dosimetry in thyroid cancer treatments using radioactive isotopes.

Finally, lung shows the longest mean free paths across all energies, consistent with its lower density. While, thyroid generally shows the shortest mean free paths, reflecting its higher atomic number content (iodine). And kidney falls between lung and thyroid in most energy ranges.

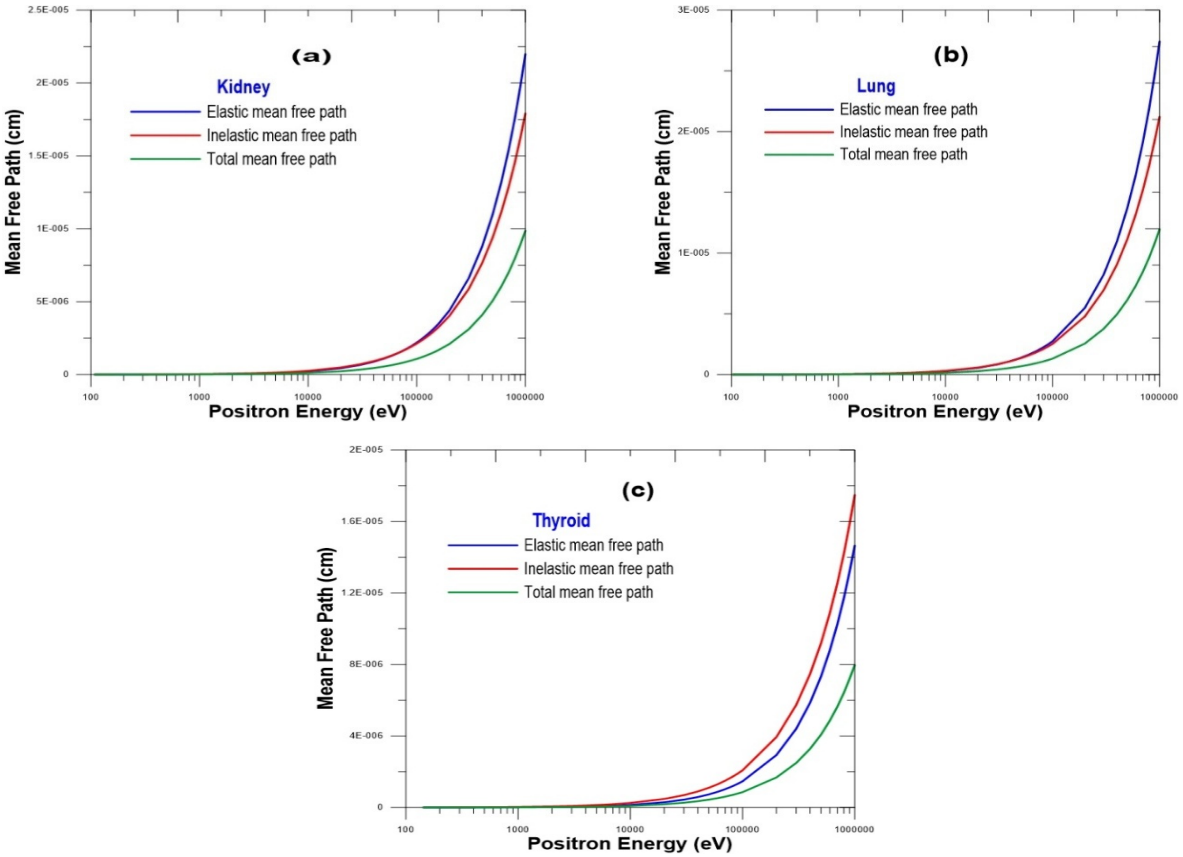

Figure 2. Calculated Elastic, Inelastic, and Total mean free paths for (a): Kidney, (b): Lung, and (c): Thyroid

5. CONCLUSIONS

In this article we presented the elastic, inelastic, total scattering cross sections for (100 eV - 1 MeV) positrons in a group of three human tissues. Also, the mean free paths of positrons are studied for the same energy ranges and human organs by the Monte Carlo method. We noted that as positron energy increases beyond 10,000 eV, all cross sections converge toward similar, very small values approaching zero. This convergence indicates that high-energy positrons interact minimally with tissue, explaining their greater penetration depth and lower stopping power at elevated energies. Conversely, material density and composition play a crucial role in determining mean free path. Higher-density materials containing more atoms and molecules increase collision probability, consequently shortening the positron mean free path, as we see in thyroid tissue [25]. It is observed from the mean free path equations, Eqs. (8) and (10), that it is inversely proportional to both the particle density and the interaction cross section.

In medical applications involving positron emitters in kidney imaging (such as PET scans), these cross sections directly influence image resolution and dose distribution. Higher cross sections at lower energies suggest that low-energy positrons interact more frequently near their emission point, potentially improving spatial resolution while increasing local dose deposition. Although a lot of models for cross section and mean free path have been discussed extensively before, rather less has been available for compound like human tissues like: kidney, lung, and thyroid because they have a complex composition.

ORCID

Hawar M. Dlshad, https://orcid.org/0000-0002-6430-8106

REFERENCES

[1] M. Danch-Wierzchowska, D. Borys, B. Bobek-Bilewicz, M. Jarzab, and A. Swierniak, "Simplification of breast deformation modelling to support breast cancer treatment planning," Biocybern. Biomed. Eng. **36**(4), 531–536 (2016). https://doi.org/10.1016/j.bbe.2016.06.001

[2] I. Adesida, R. Shimizu, and T. E. Everhart, "A study of electron penetration in solids using a direct Monte Carlo approach," J. Appl. Phys. **51**(11), 5962–5969 (1980). https://doi.org/10.1063/1.327515

[3] Y.A. Üncü, G. Sevim, O. Ağar, and H. Özdoğan, "Mass attenuation coefficient, stopping power, and penetrating distance calculations via Monte Carlo simulations for cell membranes," Kuwait J. Sci. 50(1A), 1–12 (2023). https://doi.org/10.48129/kjs.15657
[4] O.N. Vassiliev, *Monte Carlo Methods for Radiation Transport*, (Springer International Publishing, Cham, 2017). https://doi.org/10.1007/978-3-319-44141-2
[5] I. Low, and Z. Yin, "Entanglement Entropy is Elastic Cross Section," J. Med. Phys. **49**, 155–166 (2024). http://arxiv.org/abs/2410.22414
[6] K. Koç, and A. Çetin, "Investigation of Interactions Between Low Energy Positrons and DNA Using the Monte-Carlo method," NeuroQuantology, **13**(2), 160–169 (2015). https://doi.org/10.14704/nq.2015.13.2.852
[7] C.E. Chika, "Estimation of Proton Stopping Power Ratio and Mean Excitation Energy Using Electron Density and Its Applications via Machine Learning Approach," J. Med. Phys. **49**(2), 155–166 (2024). https://doi.org/10.4103/jmp.jmp_157_23
[8] C. Hugenschmidt, "Positrons in surface physics," Surf. Sci. Rep. **71**(4), 547–594 (2016). https://doi.org/10.1016/J.SURFREP.2016.09.002
[9] J.C. Ashley, "Interaction of Low-Energy Electrons with Condensed Matter: Stopping Powers and Inelastic Mean Free Paths from Optical Data," J. Electron. Spectros. Relat. Phenomena, **46**, 199–214 (1988).
[10] Z. Tan, *et al*., "Cross sections of electron inelastic interactions in DNA," Radiat. Environ. Biophys. **43**(3), 173–182 (2004). https://doi.org/10.1007/s00411-004-0249-4
[11] Z. Tan, *et al*., "Electron stopping power and mean free path in organic compounds over the energy range of 20-10,000 eV," Nucl. Instrum. Methods Phys. Res. B, **222**(1-2), 27–43 (2004). https://doi.org/10.1016/j.nimb.2004.02.017
[12] L.H. Cai, B. Yang, C.C. Ling, C.D. Beling, and S. Fung, "Monte carlo simulation of positron induced secondary electrons in thin carbon foils," Journal of Physics: Conference Series, Institute of Physics Publishing, **262**, 012009 (2011). https://doi.org/10.1088/1742-6596/262/1/012009
[13] K. Ratnavelu, M. J. Brunger, and S.J. Buckman, "Recommended Positron Scattering Cross Sections for Atomic Systems," J. Phys. Chem. Ref. Data, **48**(2), (2019). https://doi.org/10.1063/1.5089638
[14] B.P. Nigam, M.K. Sundaresan, and T.-Y. Wu, "Theory of Multiple Scattering: Second Born Approximation and Corrections to Molière's Work," Physical Review, **115**(3), 491–502 (1959). https://doi.org/10.1103/PhysRev.115.491
[15] S. Yalcin, U. Akar Tarim, O. Gurler, O. Gundogdu, and D. A. Bradley, "Screening parameter for elastic scattering of electrons," Radiation Effects and Defects in Solids, **176**(9–10), 919–939 (2021). https://doi.org/10.1080/10420150.2021.1975709
[16] M. Gryzinski, "Two-Particle Collisions. II. Coulomb Collisions in the Laboratory System of Coordinates," Physical Review, **138**(2), 322–335 (1965).
[17] M. V. Manjunatha, and T. K. Umesh, "Effective atomic number of some rare earth compounds determined by the study of external bremsstrahlung," J. Radiat. Res. Appl. Sci. **8**(3), 428–432 (2015). https://doi.org/10.1016/j.jrras.2015.03.005
[18] V. De Smet, R. Labarbe, F. Vander Stappen, B. Macq, and E. Sterpin, "Reassessment of stopping power ratio uncertainties caused by mean excitation energies using a water-based formalism," Med. Phys. **45**(7), 3361–3370 (2018). https://doi.org/10.1002/mp.12949
[19] G.S. Ibbott, "Radiation Dosimetry: Electron Beams with Energies Between 1 and 50 MeV (ICRU Report No. 35)," Med. Phys. **12**(6), 813–813 (1985). https://doi.org/10.1118/1.595780
[20] M. Grvzinski, "Two-Particle Collisions. I. General Relations for Collisions in the Laboratory System," Physical Review, **138**(2), 305–321 (1965).
[21] M. Asai, M.A. Cortés-Giraldo, V. Giménez-Alventosa, V. Giménez Gómez, and F. Salvat, "The PENELOPE Physics Models and Transport Mechanics. Implementation into Geant4," Front. Phys. **9**, 1–20 (2021). https://doi.org/10.3389/fphy.2021.738735
[22] N.J. Carron, *An Introduction to the Passage of Energetic Particles through Matter*, (Taylor & Francis Group, California, USA, 2021). https://doi.org/10.1201/9781420012378
[23] M. Dapor, "Comparison of Electron Compton Scattering with Positron Compton Scattering in Polyethylene," Materials, **18**(7), 1–10 (2025). https://doi.org/10.3390/ma18071609
[24] A. Alshibel, and K. T. Osman, "Mass Stopping Power and Range of Alpha Particles in Biological Human Body Tissues (Blood, Brain, Adipose and Bone)," OAlib, **10**(10), 1–17 (2023). https://doi.org/10.4236/oalib.1110775
[25] A.B. Denison, and H. H. Farrell, "Positron mean free paths between 50 eV and 40 keV," Phys. Rev. B: Condens. Matter. Mater. Phys. **69**(10), 1–8 (2004). https://doi.org/10.1103/PhysRevB.69.104302
[26] S.V. Stepanov, V.M. Byakov, and P.S. Stepanov, "Positronium in Biosystems and Medicine: A New Approach to Tumor Diagnostics Based on Correlation between Oxygenation of Tissues and Lifetime of the Positronium Atom," Physics of Wave Phenomena, **29**(2), 174–179 (2021). https://doi.org/10.3103/S1541308X21020138
[27] E.C. Emond, A.M. Groves, B.F. Hutton, and K. Thielemans, "Effect of positron range on PET quantification in diseased and normal lungs," Phys. Med. Biol. **64**(20), 1–16 (2019). https://doi.org/10.1088/1361-6560/ab469d
[28] H.I. Coerts, B. de Keizer, and F.A. Verburg, "Advances in the Development of Positron Emission Tomography Tracers for Improved Detection of Differentiated Thyroid Cancer," Cancers (Basel), **16**(7), 1–12 (2024). https://doi.org/10.3390/cancers16071401
[29] ICRU, "Tissue substitutes in radiation dosimetry ana measurement ICRU report 44," Bethesda, (1989).
[30] M. Kefalati, S.F. Masoudi, and A. Abbasi, "Effect of human body position on gamma radiation dose rate from granite stones," J. Environ. Health. Sci. Eng. **19**(1), 933–939 (2021). https://doi.org/10.1007/s40201-021-00660-7
[31] A. Arectout, *et al*., "Investigation of photon interaction parameters in Human Body Tissues using GAMOS, FLUKA, and XCOM Studies," Nuclear Analysis, **4**(1), 1–11 (2025). https://doi.org/10.1016/j.nucana.2024.100141
[32] P. Moskal, *et al*., "Positronium image of the human brain in vivo," Sci. Adv. **10**(37), (2024). https://doi.org/10.1126/sciadv.adp2840

КОД МОНТЕ-КАРЛО ДЛЯ РОЗРАХУНКУ ПРУЖНОГО ТА НЕПРУЖНОГО ПЕРЕРІЗУ РОЗСІЯННЯ ТА СЕРЕДНЬОЇ ДОВЖИНИ ВІЛЬНОГО ПРОБІГУ РОЗСІЯННЯ ПОЗИТРОНІВ В ОРГАНАХ НИРОК, ЛЕГЕНЬ ТА ЩИТОВИДНОЇ ЗАЛОЗИ

Хавар М. Длшад[1], Джамал М. Рашид[2]

[1]Університет Сулеймані, Коледж освіти, кафедра фізики, Сулейманія 46001, Регіон Курдистан, Ірак

[2]Університет Сулеймані, Коледж природничих наук, кафедра фізики, вулиця Клясан, Сулейманія 46001, Регіон Курдистан, Ірак

У цьому дослідженні розраховано загальні перерізи розсіювання позитронів у тканинах нирок, легень та щитовидної залози в діапазоні енергій від 100 еВ до 1 МеВ. Методи Монте-Карло були використані для визначення як пружних, так і непружних інтегральних перерізів, використовуючи формулу Резерфорда для пружного розсіювання та функцію збудження Гризінського для непружних процесів. Було проведено порівняння між пружними та пружними перерізами Пенелопи. У дослідженні також розглядалися пружна, непружна та повна довжина вільного пробігу як функції енергії позитронів для всіх трьох типів тканин. Обчислювальний підхід розроблений для широкого застосування до різних матеріалів. Ми спостерігали значні відмінності в профілях поперечного перерізу та в енергетичних залежностях довжини вільного пробігу між тканинами, пояснюючи ці варіації різними характеристиками непружного розсіювання, властивими кожному матеріалу. Хоча систематичні невизначеності в обчислювальному алгоритмі важко точно кількісно визначити, ми вважаємо, що вони значною мірою є систематичними.

Ключові слова: *поперечний переріз; позитрон; середній вільний пробіг; орган людини; ефективний атомний номер*